Antiferromagnetism in two-orbital model for $s^{\pm}$-wave iron based superconductors

P. K. Parida[1,3], B. Pradhan[2], S. Sahoo[3]

[1]Department of Physics, Dhenkanal (A) College, Dhenkanal-759001, Odisha, India
[2]Department of Physics, B.J.B. College, Bhubaneswar-751014, Odisha, India
[3]Department of Physics, NIT, Durgapur-713209, West Bengal, India

Email: parida.pkumar@gmail.com

Abstract

In iron based superconductors the superconducting phase occurs near the onset of antiferromagnetism order. Unconventional superconductivity has led to extensive experimental and theoretical studies on the effect of electron correlations and on the nature of magnetism in iron based superconductors. For the study of antiferromagnetism in these superconductors we have proposed a tight-binding two-orbital model Hamiltonian. We have proposed here a $s^{\pm}$-wave pairing symmetry of the form $cosk_x \times cosk_y$ in the model in mean-field approximation. The model is solved by Zubarev's double-time Green's function technique to find the self-consistent gap equation and is solved self-consistently numerically. The antiferromagnetism gap, specific heat, conduction electron density of states and energy band structure for the system are calculated.

Keywords: *Iron based superconductors, Antiferromagnetism, Density of states*

1. Introduction

The recent discovery of superconductivity in the iron based superconductors (FeSCs) generated enormous interest in the physics of these materials [1–4] . The origin of pairing mechanism in FeSCs is still highly debated and the topic remains one of the most important open problems in Condensed Matter Physics [5–8]. It is widely believed that the crystal structure, magnetic properties, and the degree of electronic correlation are all fundamental aspects to clarify the physics of these materials [7,9–11]. The FeSCs exhibit the common feature of phase diagrams, where parent compounds show the tetragonal to orthorhombic structural transition and the stripe type antiferromagnetism (AFM) transition both of which are suppressed by carrier doping x resulting in the high-Tc superconductivity [1,11]. When approaching the AFM transition, the AFM fluctuation observed by the NMR experiments [12] is found to be enhanced. High temperature superconductivity in these materials emerges from, or sometimes coexists with, their metallic or insulating parent compound states. Surprisingly these compounds in their undoped states exhibit dramatically different antiferromagnetism spin arrangements and Néel temperatures. Although the magnetic interactions are important for superconductivity, much remains unknown concerning the microscopic origin of the magnetic states [6]. The origin of magnetism in the iron based superconducting parent compounds is hotly debated since it is believed that the same magnetic interactions that drive the magnetic ordering also produce the Cooper pairing [13]. The phase diagram of iron based superconductors is similar to high-T_c cuprates as it contains an antiferromagnetism (AFM) phase in close proximity to the superconducting (SC) one. At low carrier concentrations most of the iron based superconductors exhibit an AFM state whose suppression with doping, pressure or disorder allows

for the emergence of superconductivity. This shows strong similarities in phase diagram with cuprate superconductors and is evidence for the interplay between magnetism and superconductivity in the FeSCs. The important properties of FeSCs are that, the parent compounds are antiferromagnetism metals and the superconducting pairing symmetry in most of the materials is an extended s-wave [13].

If we focus on metallic FeAs materials, for which the weak-coupling analysis seems to be applicable. The Neutron scattering measurements have revealed the ordering momentum in the unfolded Brillouin zone to be either (0, π) or (π , 0) i.e. the magnetic order consists of ferromagnetic chains along one crystallographic direction and antiferromagnetism chains along the other direction. The transfer of spectral weight from the Drude peak to a mid-infra-red peak observed by the optical conductivity measurements is consistent with itinerant electrons giving rise to AFM order [14]. The nesting mechanism is known to give rise to the incommensurate AFM in *Cr* [15]. The electronic structure of iron pnictides assumes the emerge of AFM order, due to near nesting between the dispersions of holes and electrons. The ab-initio analysis confirms that the total energy in the AFM state shows that the main energy gain with respect to the paramagnetic state comes from regions of the Brillouin zone where electron and hole pockets reside [16]. The rest of this paper is organised as follows. We introduce two-orbital model describing FeSCs in section 2. In section 3 we have the calculation of Green's functions and the AFM order parameter. The temperature dependence of AFM order parameter along with specific heat, density of states (DOS) and band energies are also discussed in section 4. The summary is given in Section 5.

2. Theoretical Model

The iron-based superconducting compounds share in common the basic electronic structure consisting of *Fe 3d* bands near Fermi level (FL), with the d_{xz}, d_{yz} and d_{xy} orbitals most active near FL. Considering these three active orbitals near FL, the d_{xz} and d_{yz} orbitals are bound by C_4 symmetry to be degenerate in the tetragonal state. The d_{xy} orbital, however, does not necessarily need to behave in the same way as d_{xz}/d_{yz}. Again the assumption of the crystal field splitting and the orbital hopping effect considers the d_{xz} and d_{yz} orbitals of *Fe* for low energy physics discussions [17]. With this prescription here we have considered a model Hamiltonian for the AFM interaction in the $s^{\pm}$-wave symmetry and solved self-consistently. The AFM order is characterised by the spin alignment on Fe lattice sites of FeSCs, which leads to the Néel ground state from the antiferromagnetism exchange. Due to the above reason, the *Fe* lattice is divided into two sub lattices with electron operators $c_{i,\alpha,k,\sigma}$ and $c_{j,\alpha,k,\sigma}$ for electron momentum k and spin σ. The hopping of the conduction electrons between the neighbouring sites of the two degenerate orbits of Fe^{2+} is described by the Hamiltonian H_0 as

$$H_0 = \sum_{\alpha,k\sigma} \varepsilon_k \left[\left(c^{\dagger}_{i,\alpha,k,\sigma} c_{j,\alpha,k,\sigma} + c^{\dagger}_{i,\alpha,k,\sigma} c_{j,\alpha',k,\sigma} \right) + H.c. \right] \qquad (1)$$

Here i and j represent two neighbouring sites, $\alpha = 1$ and 2 are the two JT distorted orbitals with momentum k and spin σ. The conduction electron creation (annihilation) operators are $c^{\dagger}_{i,\alpha,k,\sigma}$ ($c_{i,\alpha,k,\sigma}$) and $c^{\dagger}_{j,\alpha,k,\sigma}$ ($c_{j,\alpha,k,\sigma}$) with the square lattice nearest neighbour tight-binding hopping in the form $\varepsilon_k = -2t_0(\cos k_x + \cos k_y)$ where t_0 is the hopping integral.

The Heisenberg exchange interaction between the magnetic moments at the neighbouring sites produces the sub-lattice magnetisation. The AFM Hamiltonian within the mean field approximation for the staggered sub lattice magnetisation can be written as

$$H_{AFM} = \frac{h}{2} \sum_{\alpha,k,\sigma} s \left[c^{\dagger}_{i,\alpha,k,\sigma} c_{i,\alpha,k,\sigma} - c^{\dagger}_{j,\alpha,k,\sigma} c_{j,\alpha,k,\sigma} \right] \qquad (2)$$

Here, $s = \pm 1$ is the spin index and it is $+1$ for up and -1 for down spins respectively. The AFM order parameter h is described as

$$h = -\frac{1}{2} g_L \mu_B \sum_{\alpha,k,\sigma} s\left[\left\langle c^{\dagger}_{i,\alpha,k,\sigma} c_{i,\alpha,k,\sigma}\right\rangle - \left\langle c^{\dagger}_{j,\alpha,k,\sigma} c_{j,\alpha,k,\sigma}\right\rangle\right] \quad (3)$$

Here, g_L and μ_B are the Lande-g factor and Bohr magnetron respectively.

Here, we consider the $s^{\pm}$-wave pairing form factor as $cosk_x \times cosk_y$ [18,19]. However, it is important to realise that the $s^{\pm}$-wave gap function is not synonymous to $cosk_x \times cosk_y$. Indeed, the $s^{\pm}$-wave form factor obtained from several weak coupling approaches [20–22] has a strong variation around the electron Fermi surfaces. Hence, we cannot rule out that for different order parameters the $cosk_x \times cosk_y$ can be the leading pairing form factor.

3. Calculation of order parameters

The Zubarev's single particle double-time Green's function technique [23] is being used to calculate the Green's functions. For site i the Green's functions are defined as

$$A_1(k,\omega) = \left\langle\left\langle c_{i,\alpha,k,\sigma}; c^{\dagger}_{i,\alpha,k,\sigma}\right\rangle\right\rangle_{\omega} \quad ; \quad A_2(k,\omega) = \left\langle\left\langle c^{\dagger}_{i,\alpha,-k,\sigma'}; c^{\dagger}_{i,\alpha,k,\sigma}\right\rangle\right\rangle_{\omega}$$

$$A_3(k,\omega) = \left\langle\left\langle c_{j,\alpha,k,\sigma}; c^{\dagger}_{i,\alpha,k,\sigma}\right\rangle\right\rangle_{\omega} \quad ; \quad A_4(k,\omega) = \left\langle\left\langle c^{\dagger}_{j,\alpha,-k,\sigma'}; c^{\dagger}_{i,\alpha,k,\sigma}\right\rangle\right\rangle_{\omega}$$

The Green's functions for site j are defined as

$$B_1(k,\omega) = \left\langle\left\langle c_{j,\alpha,k,\sigma}; c^{\dagger}_{j,\alpha,k,\sigma}\right\rangle\right\rangle_{\omega} \quad : \quad B_2(k,\omega) = \left\langle\left\langle c^{\dagger}_{j,\alpha,-k,\sigma'}; c^{\dagger}_{j,\alpha,k,\sigma}\right\rangle\right\rangle_{\omega}$$

$$B_3(k,\omega) = \left\langle\left\langle c_{i,\alpha,k,\sigma}; c^{\dagger}_{j,\alpha,k,\sigma}\right\rangle\right\rangle_{\omega} \quad ; \quad B_4(k,\omega) = \left\langle\left\langle c^{\dagger}_{i,\alpha,-k,\sigma'}; c^{\dagger}_{j,\alpha,k,\sigma}\right\rangle\right\rangle_{\omega}$$

The solution of these Green's functions gives us four quasi particle energy bands calculated to be

$$\pm\omega_{1,2} = \varepsilon_k \pm \sqrt{\varepsilon_k^2 + \left(\frac{h}{2}\right)^2}. \quad (4)$$

The AFM order parameter defined in eqn.(3) is calculated to be

$$h = 4 g_L \mu_B \sum_k \left[\frac{1}{\omega_1 - \omega_2}\left(\frac{1}{e^{\omega_1/t}+1} - \frac{1}{e^{\omega_2/t}+1}\right)\right]. \quad (5)$$

The k-sum involved in eqn.(5) is converted into integral form which leads to double integrals for k_x and k_y variables in a - b plane. The summation $\sum_k = N(0)\frac{S}{(2\pi)^2}\iint dk_x dk_y$ in $FeAs$ plane with appropriate limits of integration and S is the area of the square lattice and $N(0)$ is the conduction electron density of states around Fermi surface.

4. Results and Discussion

The energy gaps in high-T_c superconductors are largely anisotropic. It has been argued that the electron correlation effect should be considered to explain the anisotropic transport properties of the general d/f valence electron system [24, 25]. To perform the numerical calculations, we have considered the total band-width of conduction band $W \approx 1.0eV \approx 10000K$. All the quantities entering in eqn.(5) are made dimensionless by dividing with total band-width W. The non-dimensional parameters are the AFM order parameter $h = h/W$, reduced temperature $t = k_B T/W$ and the AFM coupling constant $g_2 = g_L \mu_B N(0)/W$,

where the conduction electron density of state (DOS) is taken as $N(0) = 1/W$. Figure 1 shows the plots of AFM order parameter h *vs* the reduced temperature t for different values of the AFM coupling $g_2 = 0.06, 0.08, 0.10, 0.12, 0.14, 0.16$ and 0.18. The AFM gap parameter as well as the Néel temperature t_N increases with the increase of the AFM coupling. The gap parameter shows mean-field behaviour towards higher temperature. At lower temperatures the gap value is not mean-field like may be due to hybridisation effect as confirmed from specific heat plots later.

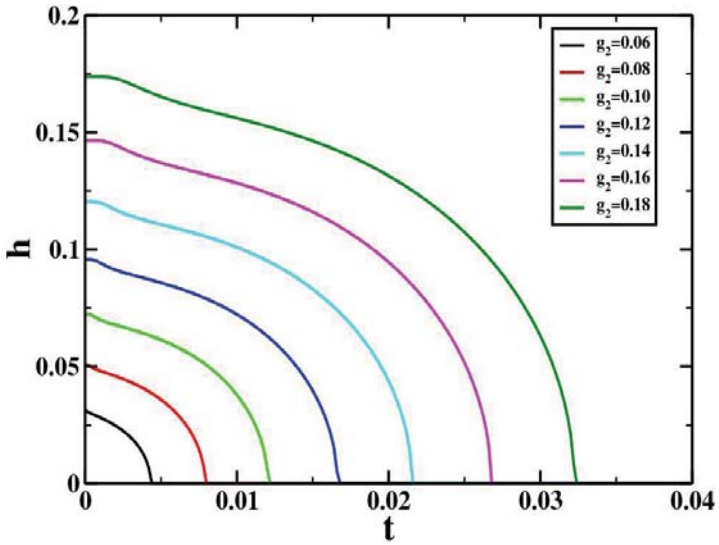

FIG 1. (Colour online) The plots of the AFM gap h *vs* reduced temperature t for different values of the AFM coupling $g_2 = 0.06, 0.08, 0.10, 0.12, 0.14, 0.16$ and 0.18.

4.1. Specific heat

In order to address the inhomogeneity in the transition, we first calculate the quasiparticle entropy S(T) according to the expression [26]

$$S(T) = -2\sum_{\omega_i>0}\left[f(\omega_i)\ln\left(f(\omega_i)\right)+ f(-\omega_i)\ln\left(f(-\omega_i)\right)\right], \tag{6}$$

where $i = 1, 2$ and $f(\omega)$ is the Fermi distribution function. In finding the electronic specific heat, we first use the specific heat capacity of the system. The temperature dependent specific heat is expressed, as a function of the entropy of the system, using the expression

$$C_v(T) = T\frac{\partial S}{\partial T}. \tag{7}$$

The Sommerfelds coefficient is determined from the specific heat as

$$\gamma = \frac{C_v}{T}. \tag{8}$$

With respect to various experiments like ARPES, NMR etc., we expect that clean $s^{\pm}$-wave superconductors should display full gap behaviour just like a standard s-wave superconductor. The

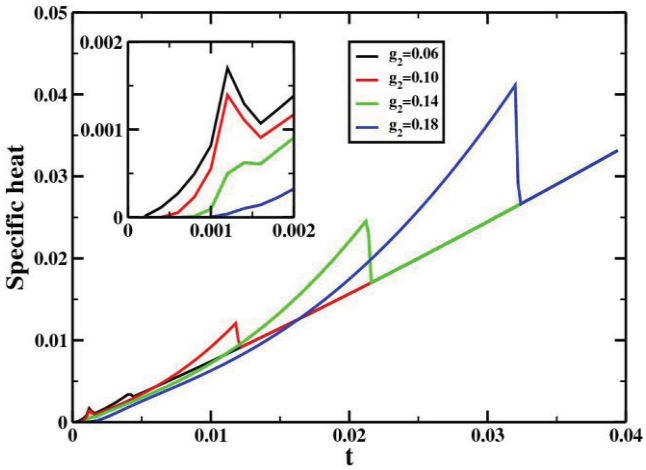

FIG 2. (Colour online) The plots of specific heat *vs* reduced temperature for different values of the AFM couopling $g_2 = 0.06, 0.10, 0.14$ and 0.18.

behaviour of iron based superconductors is in many respects consistent with BCS theory, the experimental values of C_v/T_c vary widely between different compounds, ranging between $1mJ/(molK^2)$ in under doped $Ba(Fe_{1-x}Ni_x)_2As_2$ [27] and $100mJ/(molK^2)$ in optimally hole doped $Ba_{1-x}K_xFe_2As_2$ [28–32]. Such huge variations may be partly due to differences in γ, which were indeed reported to be larger in hole doped iron based superconductors [28–33]. Figure 2 shows the temperature dependence of electron specific heat. As expected from mean-field calculations, the specific heat shows a sharp jump near the Néel temperature, separating the high temperature paramagnetic phase and the low temperature AFM phase. The sharpness of the peak near t_N shows the robust long range AFM order present in the system. However, the coefficient of electronic specific heat γ is measured to be very small, which is $0.7mJ/(molK^2)$ for AFM coupling $g_2 = 0.06$ increase upto $1mJ/(molK^2)$ with the increase of g_2 to 0.18. We observe another peak at low temperatures indicating the presence of the hybridization gap in the quasi-particle band as shown in the inset of figure 2. The hybridisation in stronger in the low AFM coupling regime as the peak diminish for higher values of this coupling.

4.2. Density of states

With an interplay of magnetic and electronic interactions likely playing an integral role in determining the shape of the phase diagram of all FeSCs. In general, these materials are two-dimensional metallic sheets with hybridised *As p*-orbitals derived from *Fe d*-states in a quasi ionic framework composed of rare earth, alkali, alkaline earth or oxygen layers. A metallic material with nominal *Fe* valence of 2^+ with low carrier concentration and high electronic density of states dominated by Fe d-states [41] are produced by this arrangement. We calculate the conduction electron density of states as follows. The imaginary part of the single-particle electron Green's functions gives the quasi-particle DOS $\rho(k,\omega,\sigma)$ which can be defined as $\rho(\omega) = \sum_{k,\sigma} \rho(k,\omega,\sigma)$. By definition $\rho(k,\omega,\sigma) = -\frac{1}{\pi}\mathrm{Im}\{G(k,\omega,\sigma)\}$, where the single particle Green's function for the conduction band is $G(k, \omega, \sigma)$ which can be found from Green's functions $A_1(k, \omega)$ and $B_1(k, \omega)$. The tunnelling conductance for iron based high-T_c superconductors [34–37] can be calculated from the quasi-particle DOS at the Fermi surface. Figure 3 shows the DOS of the conduction

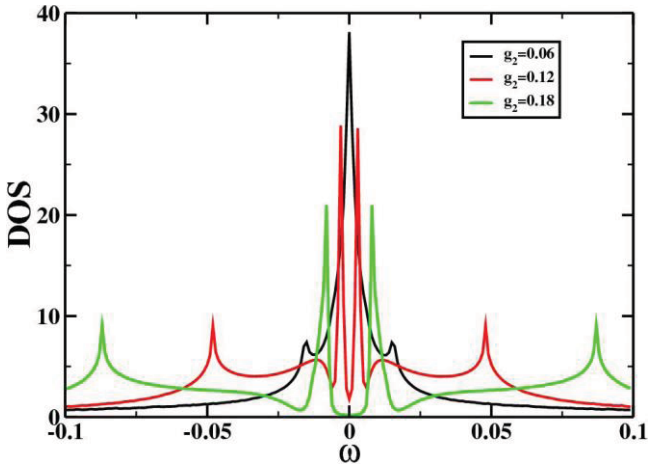

FIG 3. (Colour online) DOS plots for $h = 0.031, 0.096$ and 0.174 at $t = 0$ taking the data from figure 1 correspondig to the values of AFM coupling $g_2 = 0.06, 0.12$ and 0.18.

electrons at zero temperature for different values of AFM coupling $g_2 = 0.06, 0.12$ and 0.18. These plots show that, the AFM gap peaks appear at $\pm h/2$ with a gap around Fermi level which increases with the increase of the AFM gap. In the case of nodes imposed by symmetry, a residual DOS at zero energy is a natural consequence of the impurity scattering that broadens the nodes. However, this is not clear for the case of accidental nodes not imposed by symmetry, as in the extended s-wave case because impurity scattering will lift the nodes and produce a more isotropic gap [38, 39].

4.3. Energy Bands

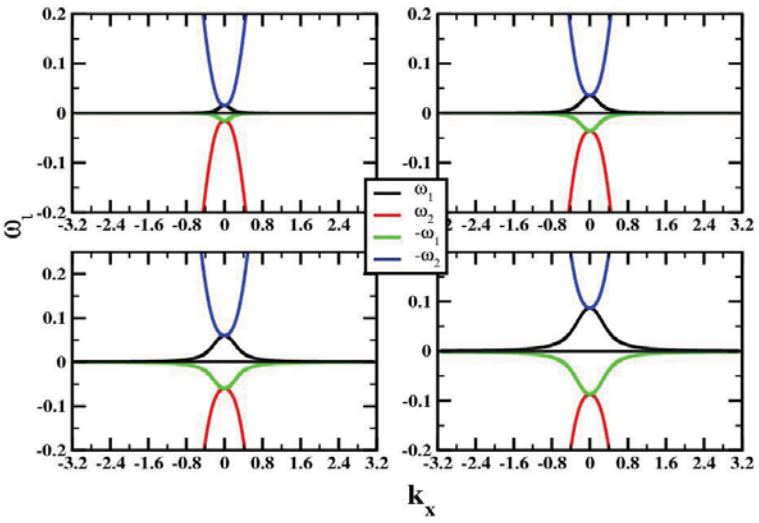

FIG 4. (Colour online)Plots of energy bands and the bare dispersion ε_k *vs* k_x for $k_y=\pi$ using parameters from figure 1 for $h = 0.031, 0.072, 0.120$ and 0.174 at $t = 0$ in (a), (b), (c) and (d) respectively.

In condensed matter physics the band theory explains the manner in which electrons in a solid behave, in the presence of each other and the surrounding ionic lattice. The band structure of a metal can convey a simple description of its electronic, optical and structural properties and is the basis for understanding many exotic phenomena. In metals, the energy states that participate in determining most properties of a material lie in close proximity to the Fermi level, the level to where available energy states are filled due to Pauli exclusion. The band structures of the FeSCs have been calculated. The dominant contribution to

the electronic density of states at FL derives from metallic bonding of the iron *d*-electron orbitals. The electronic structure and the high transition temperatures of the FeSCs suggest that the pairing interaction is of electronic origin [40]. The band structure calculations have shown that, superconductivity in FeSCs is associated with the *Fe* layer [9, 41–43]. Equation(4) describes the four energy bands for the system. We plot these bands in figure 4 for the bare energy bands and the dispersion of the solution of eqn.(4) for $k_y=\pi$. These figures show the plots of bare energy bands and the dispersion ε_k *vs* k_x for the corresponding AFM gap values at the zero temperature i.e., $t = 0$. These figures show that the energy bands at the saddle point ($k_x = 0$) are pushed away about $\pm h/2$ from the Fermi level.The hand picked values of h are taken as *0.031, 0.072, 0.120* and *0.174* at $t = 0$ from figure 1 for $g_2 = 0.06, 0.10, 0.14$ and *0.18* respectively. The corresponding plots are shown in figures 4(a), 4(b), 4(c) and 4(d) for more convenient.

5. Conclusion

In this communication, we like to study the different aspects of AFM order parameters in extended s-wave iron based superconductors by a mean-field model Hamiltonian.The AFM order parameter is calculated by Zubarev's technique of double-time electron Green's function. The AFM shows some anomalies towards the lower temperatures observed in gap parameter as well as in the specific heat and DOS studies. The hybridisation effect is clearly seen in the specific heat plots as discussed and the gap around the Fermi level in the DOS plots is due to the impurity scattering which may be of hybridisation type. The band energies show the saddle point displacement equivalent to the AFM gap value with the Fermi surface around the (π, 0) point which is in good agreement with the experimental findings.

6. Acknowledgements

The authors gracefully acknowledge the research facilities offered by the Institute of Physics, Bhubaneswar, India and Dr. B. K. Panda of Ravenshaw University, Cuttack, India for valuable discussions.

REFERENCES

[1] Y Kamihara, T Watanabe, M Hirano, H Hosono, J. American Chem. Soc. 130, 3296 (2008)

[2] M Rotter, M Tegel, D Johrendt, Phys. Rev. Lett. 101, 107006 (2008)

[3] X H Chen, T Wu, G Wu, R H Liu, H Chen, D F Fang, Nature (London) 453, 761 (2008)

[4] G F Chen, Z Li, D Wu, G Li, W Z Hu, J Dong, P Zheng, J L Luo, N L Wang, Phys. Rev. Lett. 100, 247002 (2008)

[5] P Dai, Rev. Mod. Phys. 87, 855 (2015)

[6] P Dai, J Hu, E Dagotto, Nature Physics 8, 709 (2012)

[7] E Dagotto, Rev. Mod. Phys. 85, 849 (2013)

[8] G R Stewart, Rev. Mod. Phys. 83, 1589 (2011)

[9] I I Mazin, M D Johannes, Nat. Phys. 5, 141 (2009)

[10] Q M Si, R Yu, E Abrahams, Nat. Rev. Mater. 1, 16017 (2016)

[11] D C Johnston, Adv. Phys. 59, 803 (2010)

[12] F L Ning, K Ahilan, T Imai, A S Sefat, M A McGuire, B C Sales, D Mandrus, P Cheng, B Shen, H -H Wen, Phys. Rev. Lett 104, 037001 (2010)

[13] P J Hirschfeld, M M Korshunov, I I Mazin, Rev. Prog. Phys. 74, 124508 (2011)

[14] M Nakajima, S Ishida, K Kihou, Y Tomioka, T Ito, Y Yoshida, C H Lee, H Kito, A Iyo, H Eisaki, K M Kojima, S Uchida, Phys. Rev. B 81, 104528 (2010)

[15] T M Rice, Phys. Rev. B 2, 3619 (1970)

[16] O K Andersen, L Boeri, Annalen der Physik 1, 8 (2011)

[17] Tao Li, J. Phys. Soc. Jpn. 77, 103 (2008)

[18] F Yang, H Zhai, F Wang, D -H Lee, Phys. Rev. B 83, 134502 (2011)

[19] H Zhai, F Wang, D -H. Lee, Phys. Rev. B 80, 064517 (2009)

[20] F Wang, H Zhai, Y Ran, A Vishwanath, D -H Lee, Phys. Rev. Lett. 102, 047005 (2009)

[21] S Graser, T A Maier, P J Hirschfeld, D J Scalapino, New J. Phys. 11, 025016 (2009)

[22] K Kuroki, S Onari, R Arita, H Usui, Y Tanaka, H Kontani, H Aoki, Phys. Rev. Lett. 101, 087004 (2008)

[23] D N Zubarev, Sov. Phys. Usp. 3, 320 (1960)

[24] T Yoshida, S Ideta, T Shimojima, W Malaeb, K Shinada, H Suzuki, I Nishi, A Fujimori, K Ishizaka, S Shin, Y Nakashima, H Anzai, M Arita, A Ino, H Namatame, M Taniguchi, H Kumigashira, K Ono, S Kasahara, T Shibauchi, T Terashima, Y Matsuda, M Nakajima, S Uchida, Y Tomioka, T Ito, K Kihou, C H Lee, A Iyo, H Eisaki, H Ikeda, R Arita, T Saito, S Onari, H Kontani, Scientific Report 4, 7292 (2014)

[25] H S Ji, G Lee, J H Shim, Phys. Rev. B 84, 054542 (2011)

[26] B M Anderson, A Melikyan, T S Nunner, P J Hirschfeld, Phys. Rev. B 74, 060501(R) (2006)

[27] S L Bud'ko, N Ni, P C Canfield, Phys. Rev. B 79, 220516 (2009)

[28] N Ni, M E Tillman, J -Q Yan, A Kracher, S T Hannahs, S L Bud'ko, P C Canfield, Phys. Rev. B 78, 214515 (2008)

[29] J S Kim, G R Stewart, S Kasahara, T Shibauchi, T Terashima, Y Matsuda, J. Phys.: Condens. Matter 23, 222201 (2011)

[30] Z S Wang, H -Q Luo, C Ren, H -H Wen, Phys. Rev. B 78, 140501 (2008)

[31] G Mu, H Luo, Z Wang, L Shan, C Ren, H -H Wen, Phys. Rev. B 79, 174501 (2009)

[32] P Popovich, A V Boris, O V Dolgov, A A Golubov, D L Sun, C T Lin, R K Kremer, B Keimer, Phys. Rev. Lett. 105, 027003 (2010)

[33] F Hardy, T Wolf, R A Fisher, R Eder, P Schweiss, P Adelmann, H v Löhneysen, C Meingast, Phys. Rev. B 81, 060501(R) (2010)

[34] T Berlijn, C -H Lin, W Garber, W Ku, Phys. Rev. Lett. 108, 207003 (2012)

[35] Y Zhang, L X Yang, F Chen, B Zhou, X F Wang, X H Chen, M Arita, K Shimada, H Namatame, M Taniguchi, J P Hu, B P Xie, D L Feng, Phys. Rev. Lett. 105, 117003 (2010)

[36] Y Zhang, L X Yang, M Xu, Z R Ye, F Chen, C He, H C Xu, J Jiang, B P Xie, J J Ying, X F Wang, X H Chen, J P Hu, M Matsunami, S Kimura, D L Feng, Nature Materials 10, 273 (2011)

[37] P M R Brydon, C Timm, Phys. Rev. B 80, 174401 (2009)

[38] V Mishra, G Boyd, S Graser, T Maier, P J Hirschfeld, D J Scalapino, Phys. Rev. B 79, 094512 (2009)

[39] Y Nakai, T Iye, S Kitagawa, K Ishida, S Kasahara, T Shibauchi, Y Matsuda, T Terashima, Phys. Rev. B 81, 020503(R) (2010)

[40] L Boeri, O V Dolgov, A A Golubov, Phys. Rev. Lett. 101, 026403 (2008)

[41] D J Singh, M -H Du, Phys. Rev. Lett. 100, 237003 (2008)

[42] K Haule, J H Shim, G Kotliar, Phys. Rev. Lett. 100, 226402 (2008)

[43] G Xu, W Ming, Y Yao, X Dai, S Zhang, Z Fang, Euro. Phys. Lett. 82, 67002 (2008)